Clays and Clay Minerals, Vol. 52, No. 1, 115–129, 2004.

Si-ASSOCIATED GOETHITE IN HYDROTHERMAL SEDIMENTS OF THE ATLANTIS II AND THETIS DEEPS, RED SEA

NURIT TAITEL-GOLDMAN[1,2,*], CHRISTIAN BENDER KOCH[3] AND ARIEH SINGER[2]

[1] The Open University of Israel, P.O. Box 39328 Tel Aviv, Israel
[2] The Seagram Center for Soil and Water sciences, Faculty of Agricultural, Food and Environmental Quality Sciences, The Hebrew University of Jerusalem, Rehovot, Israel
[3] Chemistry Department, The Royal Veterinary and Agricultural University Thorvaldsensvej 40, DK-1871, Frederiksberg C., Denmark

Abstract—The properties of Si-associated goethite from sediments in the Atlantis II and Thetis Deeps in the Red Sea have been investigated in order to determine the effect of Si on the mineral. Two types of morphologies dominate in most samples: multi-domain crystallites, probably due to elevated Na concentration in the initial brine from which the mineral had crystallized, and mono-domain, acicular crystals. Goethite crystals with elevated Si/Fe elemental ratios are usually smaller and poorly crystalline, exhibiting numerous crystal defects, whereas larger crystals with higher crystallinity have lower Si/Fe elemental ratios. The higher Si/Fe ratios in Atlantis II Deep goethites and the lower ratio in Thetis Deep goethites probably reflect the levels of Si concentration in the hydrothermal fluids from which goethite precipitated. At relatively low Si/Fe ratios, the major effect of Si is to retard growth of the crystallites, but only a small number of defects are formed. At high Si/Fe ratios the defect concentration affects the properties of the crystals, as observed with Mössbauer spectroscopy. The Si association with goethite affects crystallinity and crystal size as indicated by X-ray diffraction, infrared spectroscopy and high-resolution transmission electron microscopy.

Key Words—Analytical Electron Microscopy, Atlantis II Deep, Crystal Properties, High-resolution Transmission Electron Microscopy, Hydrothermal Sediments, Infrared Spectroscopy, Mössbauer Spectroscopy, Si-associated Goethite, Thetis Deep, X-ray Diffraction.

INTRODUCTION

The Thetis and Atlantis II Deeps are located in the central part of the Red Sea, along the axial rift separating the Arabian and African plates. The Atlantis II Deep (A2D) has been continuously active site since its formation. Metal cations, supplied by the venting water have precipitated as oxides, silicates, carbonates and sulfides. These sediments and the overlying stratified hydrothermal brine system have been described in numerous studies (see Taitel-Goldman and Singer, 2001; Taitel-Goldman *et al.*, 2002). Sediments from the currently inactive Thetis Deep (TD) were described by Scholten *et al.* (1991). In this study we used the generalized stratigraphic sequences of the A2D and TD proposed by Bäcker and Richter (1973) and Scholten *et al.* (1991), respectively (Figure 1). Samples of goethite as a major constituent were identified in the Central-Oxidic Zone (CO) or in the Detrital-Oxidic-Pyritic Zone (DOP) in cores from A2D, and in the Fe-facies in cores from TD.

Iron concentrations (as Fe) in the hydrothermal brine system of A2D increase with depth from 0.01 mg/kg in the RSDW to 75–81 mg/kg in the lower brine, with a minimum in the upper brine, suggesting that in this layer, both oxidation and precipitation of Fe take place (Danielsson *et al.*, 1980; Hartmann, 1985). The SiO_2 concentration is enriched from 0.7 mg/kg in RSDW to 55 mg/kg in the lower brine with a similar minimum coinciding with the minimum Fe concentration (Danielsson *et al.*, 1980, Hartmann, 1985). This suggests that SiO_2 might interfere with the formation of Fe-containing minerals.

Bischoff (1969) observed a correlation of Si with Fe oxides in the A2D and suggested that SiO_2 polymerizes and precipitates on the surface of colloidal ferric hydroxide. Butuzova *et al.* (1990) found a regular increase in structural ordering in goethite from top to bottom of sediments in the A2D and suggested this trend to be caused either by crystallization of amorphous material, or transformation from lepidocrocite. In TD, however, it was suggested that goethite formation from lepidocrocite was inhibited by the presence of amorphous silica and MnO_2 (Butuzova *et al.*, 1990). Recent investigations have shown that lepidocrocite in both Deeps are associated with Si, but to different extents (Taitel-Goldman *et al.*, 2002). Anschutz and Blanc (1995) suggested that dissolved Si is removed from the brine by precipitation in the form of clay minerals or as Si-associated Fe oxides, mainly ferrihydrite. Goethite crystallites with variable amounts of associated silica (elemental ratios of 0.098–0.142), were found in the uppermost sediments in A2D and as suspended particulate matter in the overlying brine (Taitel-Goldman and Singer, 2001). This strongly suggests that goethite can

* E-mail address of corresponding author:
nuritg@openu.ac.il
DOI: 10.1346/CCMN.2004.0520111

nucleate directly within the precipitation zone, rather than being the product of transformation from ferrihydrite. Synthetic Si-associated goethite has been produced from hydrolysis in ferric systems (Cornell and Giovanoli, 1987; Glasauer, 1995; Glasauer *et al.*, 1999) and also lately from ferrous systems under conditions similar to those currently prevailing at the brine-sea water interface in the A2D (Taitel-Goldman and Singer, 2002b).

The aim of this study was to investigate authigenic goethite in a number of samples from hydrothermal sediments of the Red Sea, and to evaluate the relationship between the properties of goethite and the amount of Si associated with the crystals. The primary approach has been to correlate structural parameters of the goethite with information from elemental analysis of the crystals.

SAMPLES AND METHODS

Samples from the Red Sea Deeps had been collected by *R.V. Valdivia* during the 'Meseda 1 and 3' cruises (for the Saudi-Sudanese Red Sea Joint Commission for Exploration of Red Sea Resources). Six cores from A2D and two cores from TD were sampled for this study. To minimize the contributions from minor admixtures, we selected 16 samples, all dominated by goethite. The samples are from the SW Passage in A2D and the NE basin in TD and their positions, stratigraphy and minor additional phases are given in Table 1.

The sample depth refers to depth below sea floor and varies from 3 m below the water-sediment interface down to almost 10 m. In the TD core, only the upper Fe-facies was sampled (Figure 1).

Table 1. Sample codes, sampling positions, core depths, stratigraphic zones, colors and additional phases identified in the goethite-dominated samples.

Sample	Deep[1,2]	Core[3,4]	Positions	Location	Depth (m)	Zone[5,6]	Additional phases	Munsell colors
GN010	A2D	500KS[3]	38°04.271′E;21°21.620′N	SW passage	4.50	CO	Si-Fe plates, round particles, lepidocrocite,	Yellowish red 5YR5/6
GN011	"	"	"	"	4.70	"	Siderite, Si-Fe plates, clays	Dark red 2.5YR3/6
GN012	"	"	"	"	4.90	"	Hematite, siderite	Red 10R4/6
GN014	"	"	"	"	5.10	"	Siderite, hematite, Lepidocrocite, plates	Red 2.5 YR5/8
GN015	"	"	"	"	5.33	"	Siderite	Yellowish brown 10YR6/8
GN027	"	"	"	"	9.00	"		Yellowish gray 2.5Y5/6
GN054	"	264KS	38°04.111′E;21°20.629′N	"	5.46	"	Hematite, siderite, lepidocrocite	Yellowish red 5YR4/6
GN069	"	"	"	"	9.16	DOP	Mn siderite	Brown 10YR4/4
GN071	"	"	"	"	9.70	"	Siderite	Olive yellow 2.5Y6/6
GN086	"	296KS	38°05.134′E;21°21.171′N	"	3.11	CO	Round particles, lepidocrocite, clay	Yellowish red 5YR5/6
GN089	"	"	"	"	3.50	"	minerals	Yellowish brown 10YR5/8
GN104	"	537KS	38°04.654′E;21°21.179′N	"	4.74	"	Siderite, Si-Fe plates	Yellowish brown 10YR5/8
GN111	"	"	"	"	7.49	"	Hematite	Strong brown 7.5YR5/6
GN145	TD	620PT[4]	37°34.96′E;22°47.69′N	NE basin	1.90	Fe facies	Hematite	2.5Y5/4
GN146	"	"	"	NE basin	2.65	"	Hematite, clay minerals	2.5Y5/4
GN180	A2D	276KS	38°04.384′E;21°21.523′N	SW passage	3.64	CO/COS	Hematite (30%), Siderite, round particles	Yellowish Red 5YR4/6
GN181	"	"	"	"	3.90	"	Hematite, round particles, Siderite	Light olive brown 2.5Y6/6
GN201	"	564KS	38°04.776′E;21°21.519′N	"	4.63	CO	Siderite, Si-Fe plates	Brownish yellow 10YR6/6
GN243	TD	728KS	37°34.74E;22°47.55N	NE basin	1.50	Fe facies	Clay minerals	Brownish yellow 10YR6/4

[1] A2D - Atlantis II Deep
[2] TD - Thetis Deep
[3] KS - Kasten cores
[4] PT - Geothermal piston cores
[5] CO, COS - Central Oxidic, Central-Oxidic-Sulfidic
[6] DOP - and Detrital-Oxidic-Pyritic Zones (Bäcker and Richter, 1973). Fe facies (Scholten *et al.*, 1991)

https://doi.org/10.1346/CCMN.2004.0520111 Published online by Cambridge University Press

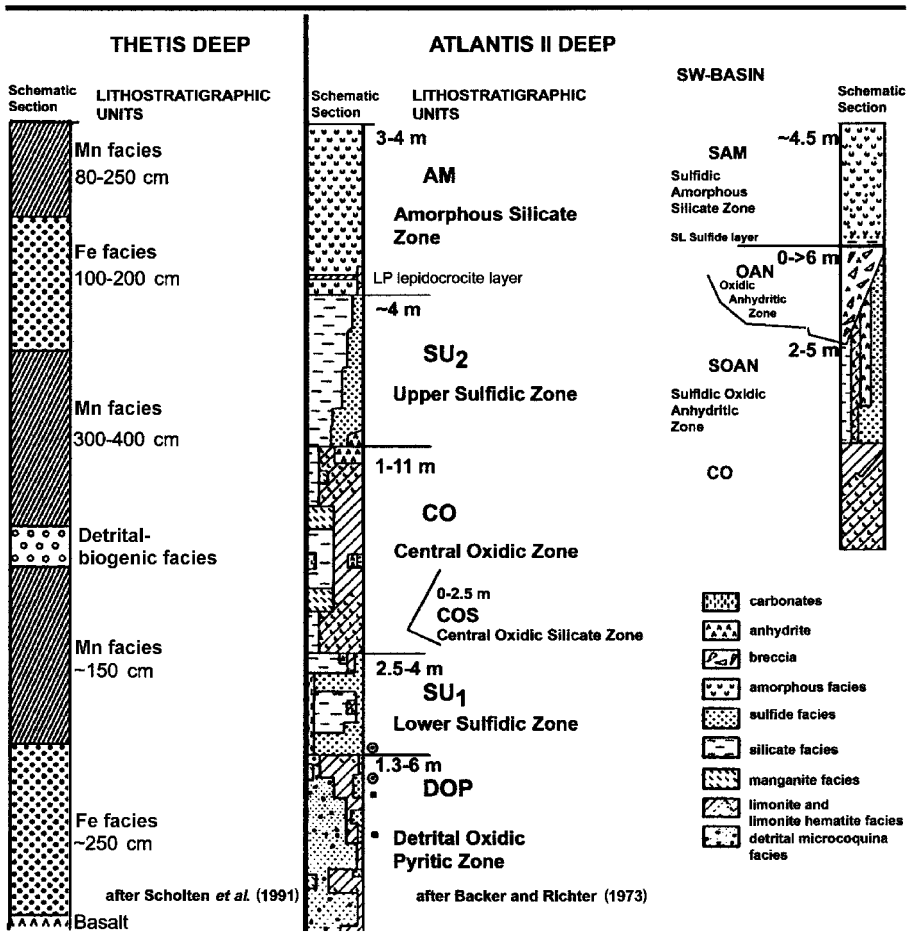

Figure 1. Lithostratigraphic scheme of Atlantis II and Thetis Deeps, Red Sea (after Bäcker and Richter, 1973, and Scholten *et al.*, 1991).

The color of moist samples was determined prior to any treatment using Munsell color classification. The detailed treatment procedure of the sample was described by Taitel-Goldman *et al.* (2002).

Phase analyses and elemental analyses by energy dispersive X-ray analysis (EDX) were carried out using a Philips EM 430 operated at 300 kV and equipped with an EDAX 9900. The particle dimensions were measured from high-resolution transmission electron microscope (HRTEM) images, summarized and presented using statistical software (SPSS). The results were plotted on a 3D diagram presenting the percentage of particle sizes within each sample and then grouped into cores and Deeps.

The XRD analyses were obtained using a Philips 1050 powder diffractometer (detailed description in Taitel-Goldman *et al.*, 2002). The mean crystallite sizes (width and thickness) of goethite were calculated from XRD line broadening, using the Scherrer formula. (As crystal length cannot be calculated from XRD pattern, it was obtained from the TEM images.)

Mössbauer spectra were measured at temperatures between 5 and 300 K (Taitel-Goldman *et al.*, 2002). For comparison of parameters, the Mössbauer spectra of a pure, well crystallized, natural goethite sample (Mørup *et al.*, 1983) were measured using the same experimental setup. The samples are grouped based on the Mössbauer spectra at low temperature: spectra of essentially goethite (with or without additional phases) and one sample strongly deviating from the ideal.

Infrared spectra were obtained using a Nicolet FTIR spectrometer (details in Taitel-Goldman *et al.*, 2002).

Three different chemical methods were used to determine the elemental composition and distribution in the samples. Ammonium oxalate (Schwertmann, 1959; Schwertmann, 1964; McKeague and Day, 1966) and DCB (dithionite-citrate-bicarbonate) (Mehra and Jackson, 1960) extractions were compared with elemental analyses of individual multi-domain crystals, and clusters of a number of crystals (Taitel-Goldman *et al.*, 2002). Significance levels were calculated using statistical software (SAS).

https://doi.org/10.1346/CCMN.2004.0520111 Published online by Cambridge University Press

RESULTS AND DISCUSSION

Elemental analyses

Most of the samples consist either of pure goethite, or goethite accompanied by small amounts of hematite, lepidocrocite, Fe carbonates (siderite or Mn-siderite), or Si-Fe plates and rounded particles (Taitel-Goldman and Singer, 2002a). The Fe oxides, Fe carbonates and clay minerals were identified using XRD, IR and Mössbauer spectroscopy, whereas the identification of Si-Fe plates and short-range ordered rounded particles was based on electron microscopy (Table 1). Elemental analyses of goethite obtained by analytical transmission electron microscope (ATEM) demonstrated that the only element with Z >5, and associated with Fe in goethite, was Si. Overall, the elemental ratios Si/Fe ranged between 0 and 0.25 in the point analyses, *i.e.* comparable to recently formed goethite (Taitel-Goldman and Singer, 2001). These direct particle-specific measurements agree quite well with the average values measured in the oxalate and DCB extractions, indicating that Si occurs associated with Fe, rather than as separate phases (Table 2). The percentage of Fe dissolved, (and expressed as FeOOH) indicates the ratio of dissolved Fe to goethite. This ratio depends both on additional phases and the purity of the goethite in the sample. In almost mono-mineralic Si-associated goethite the ratio is very close to 100, whereas in other samples, the amounts reacted are smaller, consistent with both larger amounts of additional phases and a greater content of Si associated with the goethite.

The ratio between the oxalate and DCB-soluble FeOOH varies widely (Table 2). Because of the presence of additional Fe-containing phases in the samples, the ratio should be interpreted cautiously, but the results do suggest that some samples are distinctly less reactive due to the association of Si with the Fe oxides. Sample GN011 is singled out among all the samples because it exhibits a greater reactivity against oxalate than DCB. The Si/Fe ratio determined in the oxalate and DCB extracts compare quite well for samples showing fairly high reactivity in both extractions.

Most of the samples exhibiting only moderate dissolution in oxalate, however, have significantly higher Si/Fe ratio in the oxalate extracts. This could be caused by preferential accumulation of Si at the surfaces of the crystals, assuming uniform dissolution from the surface. Most of the samples are dominated by particles much smaller than the analytical beam in ATEM, but for a few samples it was possible to obtain series of analyses of single grains in both transverse and longitudinal directions. These measurements frequently show an enrichment of Si towards the edge in comparison to the center of the crystal (*e.g.* Si/Fe molar ratios 0.074 and 0.044 at the edge and in the center, respectively (GN015)). The higher concentration of Si at the edges of the particles is consistent with thinning towards the edge

Table 2. Chemical analyses: average Si/Fe (element basis, 10 readings) determined with ATEM and analyses of the extracts after differential dissolution with oxalate and DCB.

Sample	AEM average Si/Fe (element) in		Chemical analyses (element)					
	plates	multi-domain goethite	Small crystals	Si/Fe oxalate	% dissolved as FeOOH (oxalate)	Si/Fe DCB	% dissolved as FeOOH (DCB)	Fe-oxalate/ Fe-DCB
Almost pure Si-containing goethite								
GN015		0.06±0.01	0.10±0.003	0.04±0.005	42±3	0.03±0.002	94±0.5	0.45
GN027		0.12±0.09	0.10±0.03	0.14±0.001	5±0.9	0.04±0.007	93±0.4	0.05
GN069		0.03±0.03	0.08±0.02	0.02±0.002	39±0.2	0.01±0.005	89±1	0.44
GN071		0.02±0.01	0.05±0.01	0.02±0.002	50±4	0.01±0.003	83±0.2	0.53
GN089		0.05±0.03	0.08±0.04	0.08±0.007	4±0.5	0.03±0.006	84±0.4	0.05
GN104	12.4	0.06±0.03	0.10±0.02	0.04±0.004	44±3	0.03±0.003	86±0.1	0.51
GN111		0.08±0.02	0.12±0.01	0.12±0.006	4±0.5	0.04±0.002	86±0.2	0.05
GN201		0.05±0.03	0.08±0.1	0.04±0.003	24±2	0.03±0.002	87±0.1	0.28
GN145		0.01±0.05	–	0.02±0.002	4±0.5	0.002±0.002	60±1	0.07
GN146		0.04±0.07	–	0.03±0.005	15±2	0.01±0.005	59±0.5	0.25
Almost pure Si-containing goethite with additional oxide phases								
GN010	4.5±1.02	0.14±0.06	0.5±0.01	0.05±0.002	7±1.5	0.09±0.03	66±0.5	0.11
GN012		n.m.	n.m.	0.05±0.003	68±1.4	0.07±0.002	87±0.2	0.78
GN014	0.14±0.015	0.06±0.02	0.08±0.01	0.04±0.008	66±3	0.04±0.005	84±0.2	0.79
GN054		0.09±0.03	0.13	0.08±0.01	24±1.5	n..m.	–	
GN086		0.13±0.02	0.25±0.06	0.05±0.005	32±3	0.05±0.005	74±0.2	0.43
GN180	RP-0.2±0.05	0.04±0.05	0.015±0.01	0.03±0.01	35±2	0.04±0.001	74±0.3	0.47
GN181		0.04±0.02	0.22±0.01	0.03±0.004	58±0.9	0.03±0.004	79±0.4	0.73
GN243		0.05±0.04	–	0.04±0.004	3±1	0.01±0.005	79±0.3	0.04
Goethite with composite spectra								
GN011		0.13±0.1	0.19±0.09	0.06±0.004	89±3	0.08±0.004	71±0.5	1.25

n.m.: not measured

https://doi.org/10.1346/CCMN.2004.0520111 Published online by Cambridge University Press

where specific surface area increases. The results from all samples show that the smaller crystals exhibit greater Si/Fe ratios than multi-domain crystals (Table 2).

Infrared spectroscopy

The dominance of goethite is also confirmed by the infrared (IR) spectra showing particularly intense structural OH bands (Figure 2a,b). However, intense absorption peaks related to the presence of Si in the samples (referred to as 'IR Si area' in Figure 2b) are also clearly revealed.

The peak-fitting procedure resolves the two OH-bending modes at ~890 and ~790 cm^{-1} (δOH and γOH bands) and the Fe–O symmetric stretching vibration at 630 cm^{-1} (τO band) (Figure 2b). Bands not attributable to goethite contribute to the spectrum at ~1200–900 cm^{-1}, and a shoulder at ~670 cm^{-1} can also be detected in most samples. The broad absorption band at 1200–900 cm^{-1} was resolved into two peaks in the fitting, as suggested by the shoulder at 1080 cm^{-1}, and one peak was used to fit the shoulder at 670 cm^{-1} (Figure 2b). Three peaks were used to fit the spectra of the samples from the groups with highest Si/Fe (DCB) ratios (Table 3). Based on both the mineralogical and chemical composition of the samples, the broad band with peak positions around 1000 and 1050 cm^{-1} is suggested to originate from Si–O stretching bands. Because of the association of Fe and Si as obtained from ATEM, these bands are broadly identified with Si-goethite association. In general, the position of the absorption band of Si–O is a function of the condensation of the silica network and the neighboring cation (Moenke, 1974; Cornell *et al.*, 1987). Thus, we tentatively identify the two high-wavenumber bands between 1021–1096 cm^{-1} and 1042–1191 cm^{-1} as due to polymerized Si–O, whereas both monomeric and Fe associated networks contribute to the low-wavenumber peak. Attempting to take all contributions into account, we define the 'IR Si area' as the sum of the two (or three) contributions. The various contributions will

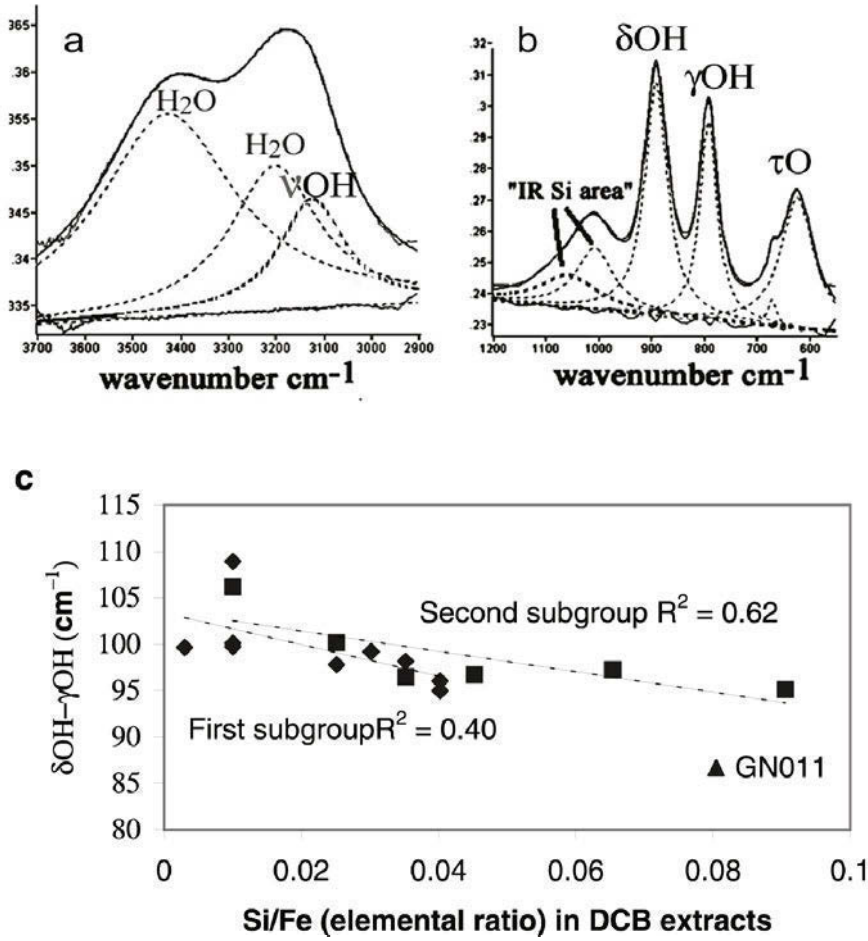

Figure 2. FTIR spectrum and correlation plots of IR parameters. (a) Sample GN027, measured FTIR spectrum and resolved bands in the 3700–2900 cm^{-1} range. (b) Sample GN015, measured FTIR spectrum and resolved bands in the 1200–550 cm^{-1} range. (c) The difference between δOH and γOH *vs.* Si/Fe in DCB extracts (R^2 = 0.40 and R^2 = 0.62 for first and second subgroups respectively. GN011 is also included). The area is measured in arbitrary units and band position in cm^{-1}.

https://doi.org/10.1346/CCMN.2004.0520111 Published online by Cambridge University Press

Table 3. Summary of the results from XRD and IR. The unit-cell parameters and crystallite sizes of goethite were evaluated using XRD. The band positions (or difference in positions) due to goethite are given together with band positions and areas of the bands assigned to Si–O (see text). The IR Si area is the sum of all the Si–O contributions.

Samples	XRD				IR											
					Goethite bands					Si bands						
	a (nm)	*b* (nm)	*c* (nm)	Mean size (nm)	νOH (cm^{-1})	δOH (cm^{-1})	γOH (cm^{-1})	δOH-γOH (cm^{-1})	τO	Position (cm^{-1})	Area	Position (cm^{-1})	Area	Position (cm^{-1})	Area	IR Si-area	Position (cm^{-1})
Almost pure Si-containing goethite																	
GN015	0.4615±0.0003	0.9967±0.0003	0.3022±0.0002	28±2	3123	891.65	792	99.65	622			1056	14.06	1007	19.17	33.23	671
GN027	0.4609±0.003	0.9967±0.0005	0.302±0.0002	28±2	3123	889	793	96	629			1082	6.71	1006	24.33	31.04	672
GN069	0.4608±0.0002	0.9966±0.0002	0.3026±0.0001	26±2	3120	894.67	794.4	100.27	624			1037	6.09	1001	1.76	7.85	671
GN071	0.4609±0.0002	0.9964±0.0002	0.3025±0.0001	28±2	3126	895.35	795.5	99.85	625			1033	4.32	998	1.29	5.61	669
GN089	0.4612±0.0003	0.9972±0.0005	0.3025±0.0002	28±2	3127	890.82	792.90	97.92	623			1053	5.25	999	7.05	12.3	668
GN104	0.4612±0.002	0.9965±0.0002	0.3022±0.0001	26±2	3126	889.47	791.44	98.03	627			1058	13.63	996	11.45	25.08	671
GN111	0.461 ±0.003	0.9971±0.0005	0.3021±0.0002	14±2	3123	885.66	789.65	96.01	628			1083	7.68	996	20.74	28.42	669
GN201	0.4613 ±0.003	0.996±0.0005	0.3021±0.0002	26.5±1.5	3130	891.94	792.63	99.31	623			1053	48.9	994	12.5	61.4	670
GN145	0.461±0.0004	0.9973±0.0007	0.3024±0.0003	39.5±2.5	3162	896.03	796.37	99.66	628			–	–	–	–	–	--
GN146	0.4609±0.0004	0.9967±0.0007	0.3024±0.0003	29±1	3151	905.03	796.1	108.93	654	1141	50.8	1076	25.91	1008	18.95	44.96	
Almost pure Si-containing goethite with additional oxide phases																	
GN010	0.461 ±0.001	0.998 ±0.001	0.3027 ±0.0005	12.5±2.5	3190	885.74	790.55	95.19	630	1191	9.46	1096	104	1021	44	157.46	676
GN012	0.462 ±0.002	0.997 ±0.002	0.302 ±0.0005	14±2	3175	885.95	788.64	97.31	636	1133	1.42	1055	18.49	1003	26.36	46.27	636
GN014	0.4616 ±0.0004	0.997 ±0.0007	0.3018 ±0.0004	24±2	3123	887.42	791.72	95.7	632			1042	16.2	993	9.07	25.27	666
GN054	0.4616 ±0.0004	0.9975 ±0.0006	0.3023 ±0.0003	12.5±2.5	3176	886	790.46	95.54	632	1121	0.36	1058	6.5	1011	38.32	45.18	
GN086	0.462 ±0.001	0.999 ±0.001	0.3025 ±0.0005	12.5±2.5	3180	884.31	788.03	96.28	632	1152	3.6	1029	70.49			74.09	670
GN180	0.462 ±0.001	0.997 ±0.001	0.3025 ±0.0005	20±2	3158	892.5	791.9	100.4	638	1125	2.9	1054	23.6	1013	29.4	11.76	669
GN181	0.4613 ±0.0001	0.9967 ±0.0002	0.3023 ±0.0001	32.5±2.5	3131	895.08	794.77	100.31	630			1066	9.5	1004	6.58	16.08	671
GN243	0.4612 ±0.0004	0.9977 ±0.0007	0.3024 ±0.0003	28±2	3140	901.3	795.05	106.25	605	1042	20.2	1021	4.25	989	1.2	25.67	673
Goethite with composite spectra																	
GN011	0.461 ±0.001	1.002 ±0.001	0.3026±0.0005	11±1	3189	873	786	87	616	1138	1.1	1034	68.33	902	7.49	76.92	

probably not have identical absorption coefficients, but we consider the area determination a good first-order proxy for the concentration of these bonds. Glasauer (1995) observed a weak absorption band around 670 cm^{-1} that related to Si association in synthetic goethite. In the present work, a small peak at the same position was also observed in several samples. The linear correlation coefficient between the area of this peak and the 'IR Si area' is $R^2 = 0.33$, with significance 0.0032 (data and plot not shown).

The position of the goethite structural OH-stretching (νOH) band was found to vary between 3120 cm^{-1} and 3180 cm^{-1}, but the significant overlap due to water hydroxyl contribution should be considered in the interpretation (Figure 2a).

The positions of the goethite bands and positions and areas for Si–O related bands are presented in Table 3. The position of the δOH band varies between 873 and 901 cm^{-1} and for γOH the position varies between 786 and 795 cm^{-1}. The value of the difference in the bending band positions varies from 87 to 106 cm^{-1}, exceeding the values reported by Cambier (1986a, 1986b). The position of τO band varies from 605 cm^{-1} to 630 cm^{-1} with most samples within the range of 620–630 cm^{-1}. The strong influence of crystallinity on the position of the bands was demonstrated by Schwertmann *et al.* (1985) and Cambier (1986a, 1986b). Based on the absence of Al, the data were searched for relations between the crystallinity and the 'activity' of Si in the samples. The Si/Fe ratio determined in the DCB extracts generally correlates quite well with the summed IR Si area ($R^2 = 0.67$ significance 0.0001, plot not shown) except for very high areas. The position of the OH-stretching band (νOH) shifts towards higher values with increasing Si/Fe ratio in DCB extracts ($R^2 = 0.41$ significance 0.006, plot not shown). Figure 2c shows the correlation plot between the difference in the positions of the bending vibrations, and the Si/Fe ratio in DCB extractions. It should, however, be simultaneously acknowledged that it is not a very strong correlation, as the samples plot more like a broad band. All available literature indicates that crystallinity is very important in determining the positions of the IR bands. However, secondary effects such as differences in the dielectric constants of the media (*e.g.* pure and Si-associated goethite), the aggregation state of the sample, the crystallite-size distributions and defects, may also contribute to scatter of the data. Environmental parameters like temperature (Cornell and Schwertmann, 1996) and elevated salinity (Taitel-Goldman and Singer, 2002b) have been shown to influence the crystallinity of goethite samples. Thus, co-variability of several of the crystallization factors within the A2D may account for some scattering of the results leading to a lower correlation coefficient. However, it appears that the major effect on crystallinity relates to the presence of Si.

X-ray diffraction

Goethite dominates the crystalline phases in the samples (Figure 3a,b,c). Some variation in unit-cell parameters were observed (a = 0.4608–0.462 nm, b = 0.996–1.002 nm and c = 0.3018–0.3027 nm) (Table 3). The present samples can be characterized as "low a-dimension" types (Schwertmann *et al.*, 1985), which previously have been found to correlate with crystallization temperatures between 40 and 80ºC. Most of the samples are characterized by an almost constant value of the b parameter (0.996–0.998 nm), but a few samples exhibit higher values (0.999–1.002 nm). These latter samples have significantly smaller mean crystalline size (width and thickness (11–12.5 nm)) compared to the other samples (12.5–32 nm), (Table 3).

In general, substitution of Fe in the cation site of goethite causes the unit-cell parameters to change. Ignoring charge effects, a hypothetical substitution of Si (IV) in octahedral coordination is expected to have a smaller radius than Fe (III) (0.040 nm *vs.* 0.064 nm) (Cornell and Schwertmann, 1996) suggesting that such a substitution would cause a contraction of unit-cell size. However, a correlation analysis of the unit-cell parameters and the average Si/Fe ratios of the crystallites indicates no systematic variation as would be expected for substitution (plots not shown).

In addition to the unit-cell parameters, mean crystallite size (width and thickness) was derived from the diffraction patterns (Table 3). The correlation plot between this mean crystallite size and the Si/Fe elemental ratio as determined by DCB extractions is shown in Figure 3d ($R^2 = 0.69$, significance 0.0001). Although a linear correlation has been used, the detailed shape of the plot indicates that the crystallite size is strongly affected at lower Si/Fe ratios (up to 0.05), whereas the crystallite size does not become smaller than ~10 nm for larger Si/Fe ratios. A study of the broadening of individual peaks as affected by Si/Fe elemental ratio yielded the following relations (Figure 3e): (1) broadening along all directions in the crystals increases with increasing Si/Fe ratios. (2) The peaks are differentially broadened, and the 110 peak is particularly affected in comparison to 020, 111 and 021. This indicates changes in the morphology of the crystallites. (3) The higher correlation coefficients were obtained for 110, 021 and 111 planes ($R^2 = 0.72$, $R^2 = 0.75$ and $R^2 = 0.70$ respectively, with significance for each correlation 0.0001), whereas 020 yielded smaller correlation coefficients ($R^2 = 0.35$, significance, 0.013). Because both IR and XRD measures of crystallinity correlate with the Si/Fe ratio, these parameters also correlate very well, indicating that, in general, both techniques measure the same concept of crystallinity. Sample GN011 appears in this plot as a single outlying point.

This finding is in line with earlier laboratory experiments in which the crystallinity of goethite was

https://doi.org/10.1346/CCMN.2004.0520111 Published online by Cambridge University Press

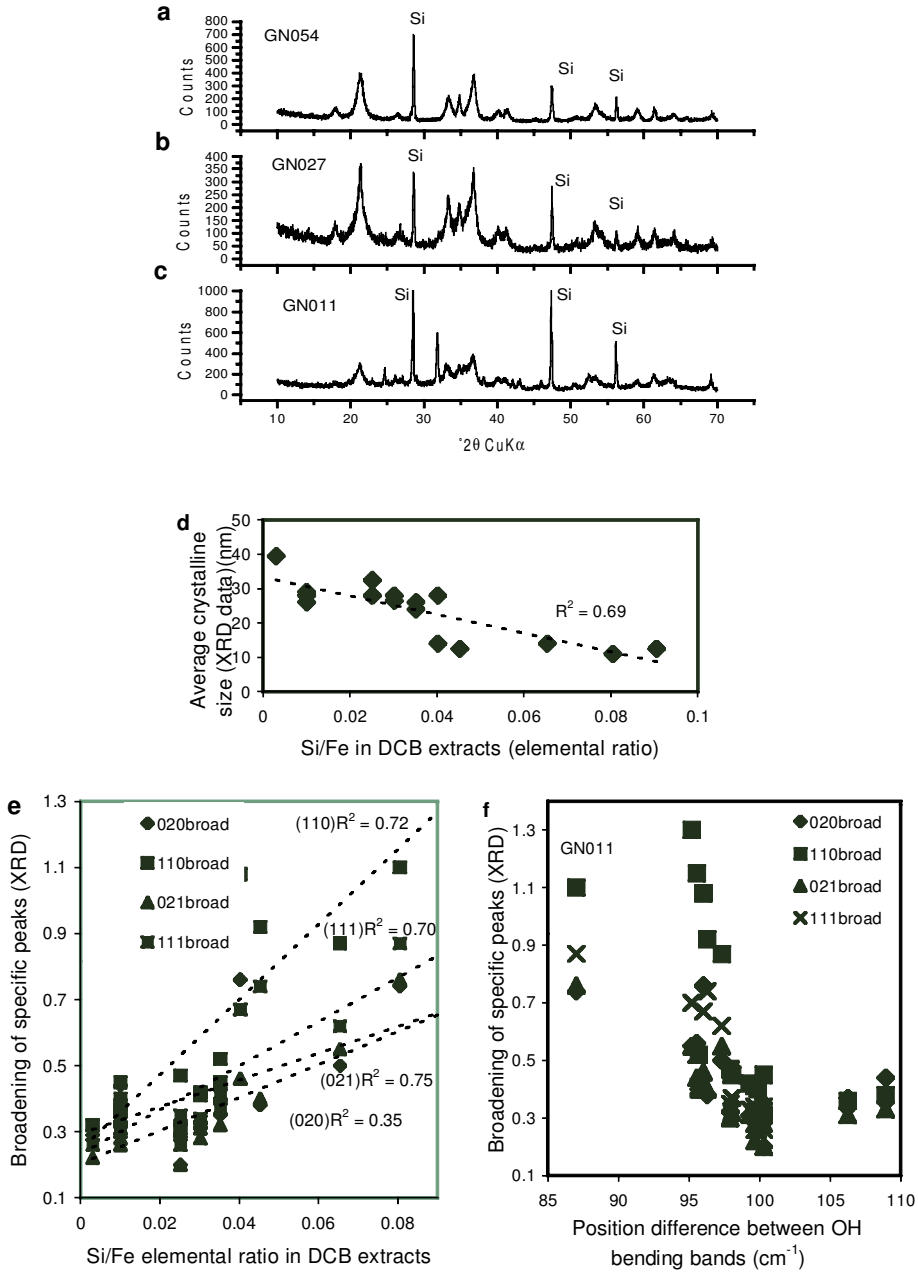

Figure 3. XRD patterns of selected samples and correlation plots: (a) XRD pattern of sample GN027; (b) XRD pattern of sample GN054; (c) XRD pattern of sample GN011; (d) mean crystallite size (width and depth) of goethite *vs*. the Si/Fe elemental ratio in the DCB extracts ($R^2 = 0.69$); (e) XRD pattern of peak broadening (FWHH – full width at half height) *vs*. the Si/Fe elemental ratio in DCB extracts (for (110) $R^2 = 0.72$; for (020) $R^2 = 0.35$; for (111) $R^2 = 0.70$ and for (021) $R^2 = 0.75$); (f) FWHH *vs*. the difference between δOH and γOH.

affected by the presence of Si during crystallization, but no indication of Si substituting for Fe was detected (Quin *et al.*, 1988; Glasauer, 1995; Glasauer *et al.*, 1999). It has been shown that at higher Si/Fe ratios, the crystallization rates decrease, causing inhibition of crystal growth (Cornell *et al.*, 1987). Cornell and Schwertmann (1996) suggested that adsorption of silicate on the terminal (021) planes of the crystals retards growth and enhances the development of these surfaces at the expense of the (110) surfaces. The natural Si-associated goethite in this study shows that Si retards crystallite growth in all directions, but with the major effect on the (110) plane and the (020) surfaces along the *c* direction. The terminal planes are less affected.

https://doi.org/10.1346/CCMN.2004.0520111 Published online by Cambridge University Press

High-resolution transmission electron microscopy

Morphology. The goethite crystals display acicular morphology, ranging in length from a few nanometers up to 1100 nm in A2D, and up to 2200 nm in TD. The majority of the particles are just a few nanometers wide and the broader ones display multi-domain characteristics.

The statistics of the crystal-size data allow for grouping of the samples (Figure 4a–d). Two size-groups dominate the samples: a group of small-sized individual crystals and a second group that is made of large multi-domain crystals of goethite elongated along the *c* direction. The crystal-size distribution patterns are related to the core site, *i.e.* mainly small crystals were found in core 500 KS (Figure 4a), whereas multi-modal size-distribution patterns characterize goethite in core 264KS (Figure 4b). Summing up all samples from A2D (Figure 4c), a bimodal size-distribution pattern appears. In the Thetis Deep, however, mainly large particles were found (Figure 4d).

The individual crystals usually have well developed, smooth faces but sometimes a rough surface is observed (Figure 5a). Different characteristic growth forms were observed in the samples. Multi-domain crystals generally 'grow' from common nuclei and then diverge. They are relatively thicker in the center and become thinner towards the edges (Figure 5b). Twinned multi-domain crystals are common (Figure 5c) and star-like twinning was also observed (Figure 5d). The widths of multi-domain crystals attain 100 nm, while individual domains are 10–20 nm wide. The multi-domainic crystals usually display well developed (110) faces and some of them terminate in well developed (021) faces (Figure 5e). Sample GN011 is singled out with respect to morphology, being dominated by small (<10 nm) mono-domain crystals almost square in projection. A few multi-domainic elongated crystals were also found in this sample (Figure 5f).

Laboratory experiments showed that high concentrations of $NaNO_3$ at elevated pH (11–12) increased the formation of multi-domainic crystals (Cornell and Giovanoli, 1986). The nucleation of domains appears to be related to the initial stages of goethite formation. Multi-domainic crystals consist of almost parallel intergrowths that emanate from a central nucleus and grow along the *z* axis. Similar conditions could possibly be related to the formation of multi-domainic goethite in these samples as present Na concentrations range from 46.9 g/kg in the upper brine up to 92.6 g/kg in the lower

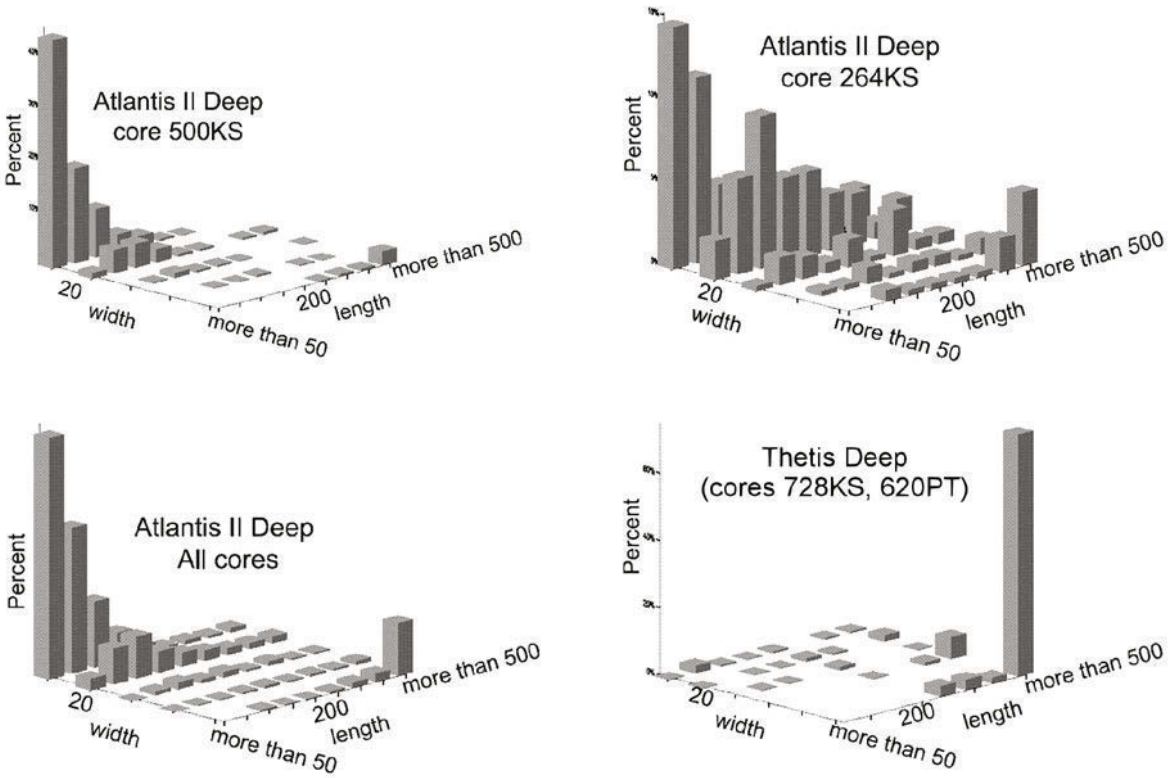

Figure 4. Size groups of goethites as observed by TEM: (a) A2D Core 500KS (samples: GN010, GN011, GN012, GN014, GN015 and GN027); (b) A2D Core 264KS (samples: GN054, GN069 and GN071); (c) all of A2D samples; (d) TD cores 728 (GN243) and 620PT (GN145, GN146). Width and length were measured in nm.

https://doi.org/10.1346/CCMN.2004.0520111 Published online by Cambridge University Press

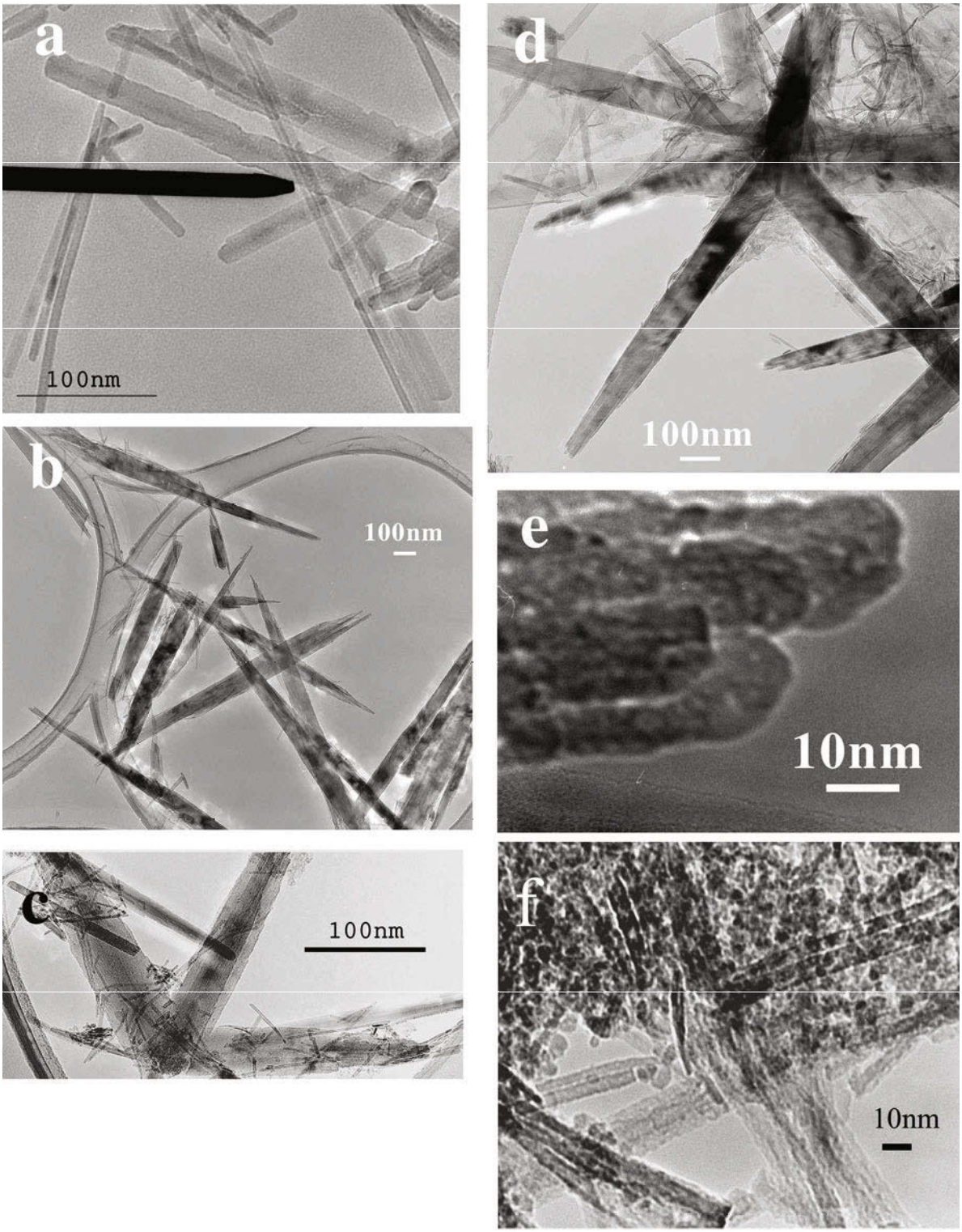

Figure 5. TEM images of goethite: (a) crystals with well developed faces along with crystals with surface roughness (sample GN071); (b) multi-domain goethite with a thickening of the central part (Sample GN243); (c) twinned multi-domain goethite (sample GN014); (d) star-like multi-domain goethite (sample GN180); (e) well developed (021) faces (sample GN054); (f) small mono-domainic square crystallites with some multi-domain crystals (sample GN011).

https://doi.org/10.1346/CCMN.2004.0520111 Published online by Cambridge University Press

brine (Brewer and Spencer, 1969). Similar Na concentrations probably prevailed during sedimentation of the CO and DOP facies.

Cornell and Giovanoli (1987) found that terminal faces ((021), (111), (121)) of goethite were especially well developed when precipitation took place in the presence of Si. They suggested that Si would adsorb particularly well to these surfaces due to a higher density of Fe atoms. The adsorbed species slow the growth and hence these faces would dominate. These experimental results can explain the elevated Si/Fe ratio at the edges of the goethite crystals from the Red Sea Deeps and the distinct (021) faces in some of the goethite. This plane has the least broadening in XRD patterns and correlates relatively strongly with the Si/Fe ratio (Figure 3e).

The frequent observation of twinned multi-domain goethite and star-like goethite in the Red Sea samples may be attributed to crystallization at elevated temperatures (60–90ºC) (Schwertmann *et al.*, 1985). Temperature increases up to 90ºC do not reduce the percentage of multi-domain crystals (Cornell and Giovanoli, 1986). At elevated temperatures (125–180º), multi-domain goethite can recrystallize into a mono-domain crystal (Schwertmann *et al.*, 1985). Thus, the common twinned multi-domain goethite found in this study, and the absence of recrystallized mono-domain goethite, set limits for the temperature range during the crystallization of most of the goethite and it also makes recrystallization under elevated temperatures less likely.

Lattice image. Lattice images of goethite are presented in Figure 6. Many crystals show high crystallinity with a low concentration of dislocations (Figure 6b) (arrow: point analysis Si/Fe = 0.015). The domains present coherent lattice images and preserve the original lattice fringes after divergence (Figure 6c). The number of dislocations observed increases with increasing Si/Fe ratios in the crystal (Figure 6d,e) (Si/Fe = 0.055). The Si/Fe elemental ratio (0.08) in sample GN011 is accompanied by numerous dislocations and the well developed (021) plane (Figure 6f,g).

Mössbauer spectroscopy

Mössbauer spectra were measured at temperatures between 5 and 300 K to ensure detailed information on the dominant goethite and allow the evaluation of possible interference on the crystallographic properties and parameters of goethite from minor phases in some of the samples. The spectra measured at room temperature of samples from the two major groups are all characterized by a dominance of magnetically ordered sextets (Table 4), indicating relatively large and chemically

Table 4. Hyperfine parameters determined from Mössbauer spectroscopy (magnetic hyperfine field B_{hf} and linewidth of at half maximum of lines 1 and 6 (FWHM) of the goethite spectra at 15 K. (Sample GN011 also at 5 K). A qualitative description of the goethite spectrum at RT is also included.

Samples	Magnetic hyperfine field B_{hf}, T ±0.3 T	FWHM, mm/s ±0.02	Component in the RT spectrum
Almost pure Si-containing goethite			
GN015	50.6	0.38	Sextet/(doublet)
GN027	50.2	0.41	Sextet/(doublet)
GN069	50.9	0.38	Sextet
GN071	50.1	0.38	Sextet
GN089	50.3	0.40	Sextet/(doublet)
GN104	50.5	0.41	Sextet/(doublet)
GN111	50.2	0.40	Sextet/(doublet)
GN145	n.m.	n.m.	Sextet
GN146	49.8	0.50	Sextet
GN201	50.3	0.40	Sextet/(doublet)
Almost pure Si-containing goethite with additional oxide phase			
GN010	50.0	0.45	Sextet/doublet
GN012	50.2	0.65	Sextet
GN014	50.6	0.39	Sextet
GN054	50.0	0.55	Sextet
GN086	50.3	0.44	Doublet/sextet
GN180	50.4	0.50	Sextet
GN181	50.4	0.37	Sextet/(doublet)
GN243	50.3	0.44	
Samples of goethite with composite spectra			
GN011	49.6	0.82	Doublet
GN011(5K)	50.0	0.74	

n.m.: not measured

https://doi.org/10.1346/CCMN.2004.0520111 Published online by Cambridge University Press

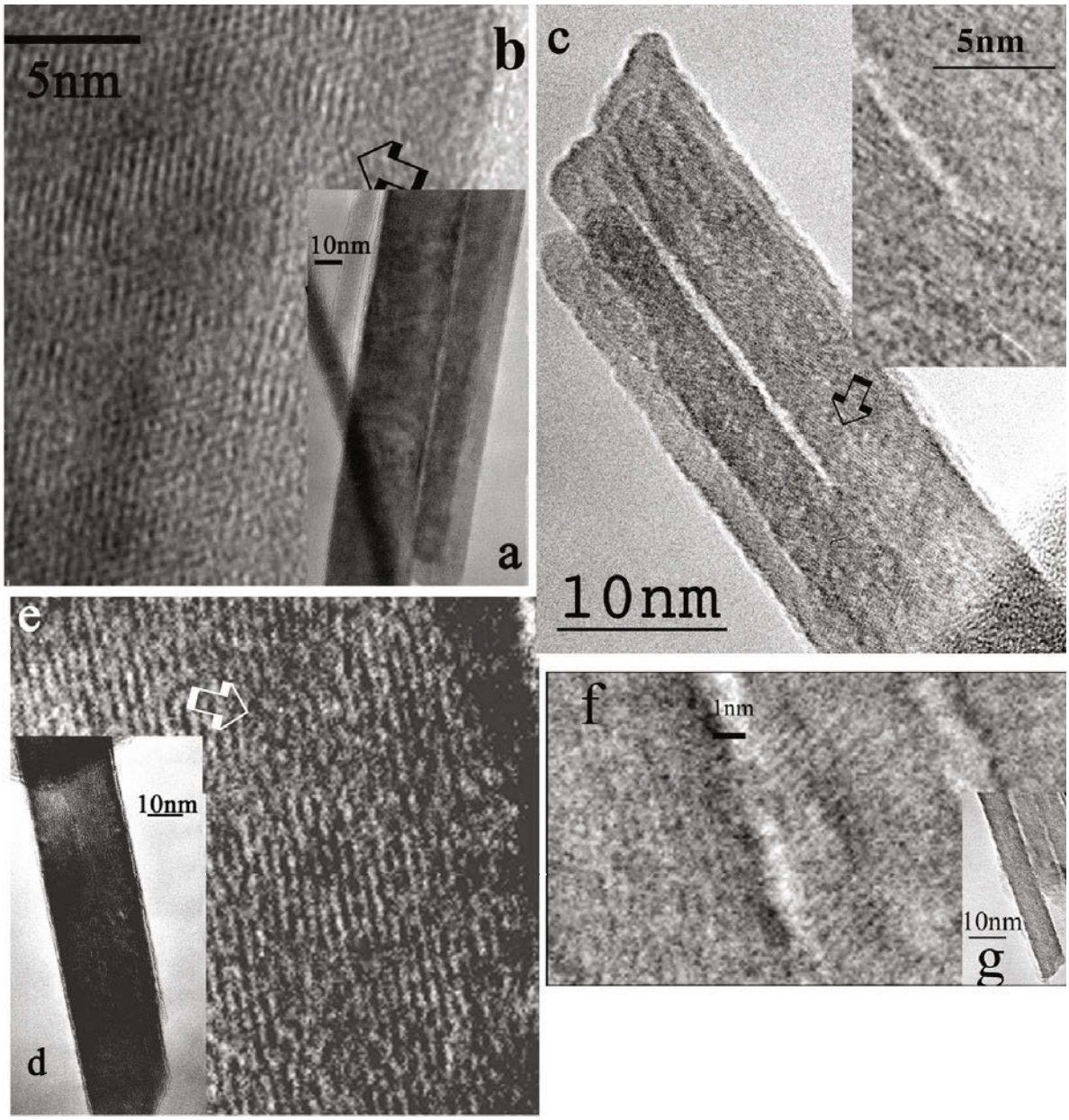

Figure 6. TEM and HRTEM images: (a) goethite multi-domain crystal; (b) HRTEM image of a goethite crystal in sample GN069 (Si/Fe = 0.015). Lattice fringes at 0.42 nm correspond to 110 spacing (arrow indicates defects in the crystal due to dislocations); (c) HRTEM image of goethite crystals in sample GN181, with preservation of lattice fringes after divergence (arrow indicates the location of the HRTEM image); (d) mono-domainic goethite in sample GN111 (Si/Fe = 0.055); (e) HRTEM image of the same crystal (arrow indicates dislocations); (f) HRTEM image of multi-domain goethite with numerous dislocations GN011 Si/Fe = 0.08; (g) TEM image of the same crystal as in f demonstrating a well developed terminate plane.

pure, well crystallized crystallites. Two samples deviate from this general pattern: GN086 and GN011 both exhibiting substantial doublets. Spectra measured at 15 K and the corresponding hyperfine parameters of goethite in the samples (magnetic hyperfine fields and line widths) are presented in Table 4. At this temperature, pure goethite exhibits a magnetic hyperfine field of 50.5 T and a line width of 0.28 mms^{-1}, which, as expected, is very close to the values found at 5 K (Mørup *et al.*, 1983). All the present samples exhibit invariant values of isomer shifts (0.48 mms^{-1} ±0.02 mms^{-1}) and quadrupole shifts (−0.12 mms^{-1} ±0.02 mms^{-1}). The samples have been grouped according to the magnetic hyperfine field at 15 K. In the first group of samples, the hyperfine field is within the measurement uncertainty identical to pure goethite.

https://doi.org/10.1346/CCMN.2004.0520111 Published online by Cambridge University Press

However, a significant broadening of the lines can be detected (0.38–0.41 mms^{-1}). This broadening cannot be explained by the presence of the minor additional phases that are primarily Fe carbonates. In the second group of samples, the hyperfine field of the goethite is also very close to pure goethite, but for a number of samples in this group it is evident that other Fe oxides are present in the samples. This might influence the fitting parameters, *e.g.* in fitting of the spectrum of GN010 a second sextet is included to account for a small amount of lepidocrocite. Because of overlap between the two sextets, the result may be slightly influenced and thus less accurate – in particular, the line width may be affected. Accordingly, the line broadening of samples from the second group (0.39 to 0.65 mms^{-1}) may also be influenced by parameters not related to goethite. Overlap with the sextets due to hematite is in general smaller, but for sample GN012 it is substantial due to reduction of the hyperfine field of hematite (presumably caused by association with Si) in this sample. Sample GN011 constitutes a group of its own based on both the reduction in hyperfine field and the increased line width. Because of the low ordering temperature of this sample, it was also measured at 5 K, demonstrating a slight increase in the hyperfine field and decreasing line width (Table 4). We consider that the hyperfine parameters at this temperature are unaffected by relaxation effects, *i.e.* they reflect the intrinsic structural disorder.

Excluding sample GN011 from the data due to dynamic effects, we have correlated the magnetic hyperfine field and Si/Fe ratios for samples in the first two groups of samples (not shown). This plot does not indicate any major influence of the Si on the hyperfine field. Likewise, the broadening of the lines appears uncorrelated with the Si association. Quin *et al.* (1988) examined Si-associated goethites and concluded that Si did not substitute for Fe in the structure, but that high Si concentrations might have prevented the formation of goethite. They thus inferred a strong adsorption of Si onto crystal growth sites. Glasauer (1995) reported that the hyperfine field at 4.2 K was almost unaffected (50.1 T, 50.2 T, 50.1 T, 50.1 T and T 49.8) by increased Si/Fe ratios (0.003, 0.02, 0.04 and 0.05, respectively). Thus, similar to XRD results, the Mössbauer investigations imply rather pure crystals in most of the samples. GN011 is an exception in this respect. The one directly observable difference between this and the other samples is the considerable number of defects observed in the TEM. Defects in oxide crystals are very difficult to observe by XRD because of their localized and random occurrence. In addition, they cause only subtle changes in the structure at the defect itself as shown by HRTEM (Figure 6f). The magnetic behavior of the structure depends, however, on highly localized interactions. Introduction of the defects will arguably weaken the interactions along a large number of super-exchange pathways at one time, causing a lowering of the hyperfine field for the Fe atoms closest to the defect. If this defect is rather random, this will not produce clearly resolved components, but rather cause broadened lines with smaller fields. Thus we propose that Si-induced defect formation at low concentrations (goethite in the first two groups) is a significant contributor to the line broadening. At high defect concentrations the ordering temperature and the low-temperature maximum hyperfine field might also become significantly affected as found in sample GN011.

Formation process

Unit-cell parameters and twinned or star-shaped goethite indicate that crystallization of goethite occurred at elevated temperatures (40–90ºC). The common multi-domainic character probably reflects crystallization under conditions of elevated Na concentration. Thus, morphology appears to be consistent with precipitation within the brine.

Precipitation of CO and DOP zones occurred during less active venting in the Deep, in a period of restricted existence of brine pools (Shanks and Bischoff, 1980). The Si-associated goethite from these zones represents precipitation under local mixing between restricted brine pools and RSDW. The Si/Fe ratios in these samples vary among core sites (*i.e.* cores 500KS and 264KS) and even within the same sedimentary core without changes that can be related to core depth. In sites with elevated Si concentrations, in agreement with Si association by the goethite, small crystals dominate, whereas lower Si concentrations enabled a larger diversity in size groups, including some larger crystals. It is suggested that the variability in Si/Fe ratios in the goethites reflect fluctuations in the chemistry of the venting brine (crystallization conditions) rather than a diagenetic recrystallization within the sediments.

In most of the samples of A2D, two crystal forms of goethite coexist: multi-domainic large crystals and smaller individual crystals. Multi-domain larger crystals with low Si/Fe ratio presumably crystallized at lower Si concentration in higher parts of the brine, whereas small crystals were formed at elevated concentrations of Si in lower parts of the mixing column. The co-existence of these two morphologies can possibly partly result from different settling velocities of the various sizes.

In the TD, only multi-domain large crystals of goethite were found. Elevated Na concentrations in the brine that filled the Deep might have encouraged the growth of multi-domain large crystals. The absence of small crystals of goethite in this Deep probably results from lower Si/Fe ratio in the hydrothermal fluids. A similar difference in the chemistry of the hydrothermal fluids is indicated by the relatively smaller Si/Fe ratios reported in lepidocrocite from TD (Taitel-Goldman *et al.*, 2002).

Both the multi-domainic and the small crystals exhibit relatively large surface areas, enabling increased

association of Si and resulting in elevated Si/Fe ratios in the precipitates. The Si is expected to precipitate on the large surfaces of the domains first as a mono-layer that at elevated Si/Fe ratios might polymerize on the surface. Small crystals have a high specific surface area, providing a larger number of precipitation sites for Si and increasing the Si/Fe ratio measured in small crystals.

The association of Si with Fe oxides should be considered in calculations involving mass balances within the brine and the sediments derived from it. It has been noted in previous works that the association of Fe and Si resulted mainly in the formation of Fe-rich clay minerals in A2D (Hartmann, 1985; Cole, 1988), or possibly Si-enriched ferrihydrite (Anschutz and Blanc, 1995). It appears, however, that Si is closely associated with the precipitation of Fe oxides either as a short-range ordered phase (Taitel-Goldman *et al.*, 1999), or as well crystallized Fe oxides (Taitel-Goldman and Singer, 2001; Taitel-Goldman *et al.*, 2002). The co-precipitation of Si with Fe oxides constitutes an important Si sink in the A2D and to a lesser extent in TD.

CONCLUSIONS

Goethite samples found in the CO and DOP zones in the A2D and in the Fe-facies in TD have Si associated with their crystals that affect their properties to various extents. They formed small individual mono-domain crystals or multi-domain, relatively large crystals that are probably induced by high Na concentrations in the brine. The Si association affects crystal morphology and size: smaller goethite crystallites and larger crystals elevated and reduced the Si/Fe ratios, respectively. Small Si/Fe ratios suggest that part of the Si is located on goethite surfaces, whereas at higher Si/Fe ratios, polymerization of the Si may occur.

No evidence for Si substitution for Fe in the structure was found, but the crystal properties of goethite are significantly affected by the presence of the Si-broadening of XRD peaks, as well as weakening of H bonds as reflected in IR spectra, and enhancement of OH-bending band separation. Mössbauer spectroscopy reveals evidence for structural disorder affecting magnetic properties.

Fluctuations in the chemistry of the venting fluids probably determine the Si/Fe in the brine and this is reflected in the goethite properties. The size of the goethite crystals and their crystallinity are the result of local crystallization environments rather than an evolutionary diagenetic pattern. The Si/Fe ratio is site-dependent, reflecting precipitation in local submarine brines with limited mixing. Their temperature was ~60–70ºC (similar to the current conditions in the A2D), hot enough to form twinning. The hydrothermal brine in TD had elevated Na concentration but lower Si concentration and probably lower temperature (<60ºC), indicating less interaction with hot rock underneath.

ACKNOWLEDGMENTS

Thanks are due to Prof. Stoffers from the Paleontologische und Mineralogische Institute in Kiel, Germany for supplying the samples; to Mr Henschel from the Technical University of Denmark for his technical assistance with the HRTEM analyses, to Dr Mogilyanski from Ben Gurion University, Israel for the XRD analyses, to Z. Hochman from the Hebrew University of Jerusalem for her technical assistance and to A. Gath, M. Zuker and Y. Abelson from the Open University Israel for their help with the statistical analyses.

REFERENCES

Anschutz, P. and Blanc, G. (1995) Geochemical dynamics of the Atlantis II Deep, Red Sea: Silica behavior. *Marine Geology*, **128**, 25–36.

Bäcker, V.H. and Richter, H. (1973) Die rezente hydrothermal-sedimentäre Lagerstätte Atlantis II Tief im Roten Meer. *Geologische Rundschau*, **Bd 62**, 697–737.

Bischoff, J.L. (1969) Red Sea geothermal brine deposits: Their mineralogy, chemistry and genesis. Pp 368–401 in: *Hot Brines and recent Heavy Metal Deposits in the Red Sea* (E.T. Degens and D.A. Ross, editors). Springer-Verlag Berlin, Heidelberg, New York.

Brewer, P.G. and Spencer, D.W. (1969) A note on the chemical composition of the Red Sea brines. Pp 174–179 in: *Hot Brines and Recent Heavy Metal Deposits in the Red Sea* (E.T. Degens and D.A. Ross, editors). Springer-Verlag Berlin, Heidelberg, New York.

Butuzova, G.Yu., Dritz, V.A., Morozov, A.A. and Gorschkov, A.I. (1990) Processes of formation of iron-manganese oxyhydroxides in Atlantis II and Thetis Deeps in the Red Sea. *Special Publications of the International Association of Sedimentology*, **11**, 57–72.

Cambier, P. (1986a) Infrared study of goethites of varying crystallinity and particle size: I: Interpretation of OH and lattice vibration frequencies. *Clay Minerals*, **21**, 191–200.

Cambier, P. (1986b) Infrared study of goethites of varying crystallinity and particle size: II: Crystallographic and morphological changes in series of synthetic goethites. *Clay Minerals*, **21**, 201–210.

Cole, T.G. (1988) The nature and origin of smectite in the Atlantis II Deep, Red Sea. *The Canadian Mineralogist*, **26**, 755–763.

Cornell, R.M. and Giovanoli, R. (1986) Factors that govern the formation of multi-domainic goethites. *Clays and Clay Minerals*, **34**, 557–564.

Cornell, R.M. and Giovanoli, R. (1987) The influence of silicate species on the morphology of goethite (α-FeOOH) grown from ferrihydrite ($5Fe_2O_3 \cdot 9H_2O$). *Journal of the Chemical Society, Chemical Communications*, 413–414.

Cornell, R.M. and Schwertmann, U. (1996) *The Iron Oxides, Structure, Properties, Reactions, Occurrence and Uses*. VCH Verlagsgesellschaft mbH Weinheim, Germany, 573 pp.

Cornell, R.M., Giovanoli, R. and Schindler, P.W. (1987) Effect of silicate species on the transformation of ferrihydrite into goethite and hematite in alkaline media. *Clays and Clay Minerals*, **35**, 1 21–28.

Danielsson, L.G., Dyrssen, D. and Graneli, A. (1980) Chemical investigation of Atlantis II and Discovery brines in the Red Sea. *Geochimica et Cosmochimica Acta*, **44**, 2051–2065.

Glasauer, S.M. (1995) Silicate Associated with Fe(hydr)oxides. Dissertation, Technische Universität Munchen, Germany, 134 pp.

Glasauer, S., Friedl, J. and Schwertmann, U. (1999) Properties of goethites prepared under acidic and basic conditions in

the presence of silicate. *Journal of Colloid and Interface Sciences*, **216**,106–115.

Hartmann, M. (1985) Atlantis-II Deep brine system. Chemical processes between hydrothermal brine and Red Sea deep water. *Marine Geology*, **64**, 157–177.

McKeague, J.A. and Day, J.H. (1966) Dithionite- and oxalate-extractable Fe and Al as aids in differentiating various classes of soils. *Canadian Journal of Soil Science*, **46**, 3–22.

Mehra, O.P. and Jackson, M.L. (1960) Iron oxides removal from soils and clays by dithionite-citrate system buffered with sodium bicarbonate. Pp. 317–327 in: *Proceedings of the 7th National Conference of the Clay Minerals Society*, Washington, D.C., 1958 (A. Swineford, editor). Pergamon Press, New York.

Moenke, H.H. (1974) Silica, the three dimensional silicates, borosilicates, and beryllium silicates. Pp. 365–382 in: *The Infrared Spectra of Minerals* (V.C. Farmer, editor). Monograph **4**, Mineralogical Society, London.

Mørup, S., Madsen, M.B., Franck, J., Villadsen, J. and Koch, C.J.W. (1983) A new interpretation of Mössbauer spectra of microcrystalline goethite: "super-ferromagnetic" or "super-spin glass" behavior? *Journal of Magnetism and Magnetic Materials*, **40**, 63–174.

Quin, T.G., Long, G.J., Benson, C.G., Mann, S. and Williams, R.J.P. (1988) Influence of silicon and phosphorus on structural and magnetic properties of synthetic goethite and related oxides. *Clays and Clay Minerals*, **36**, 165–175.

Scholten, J.C., Stoffers, P., Walter, P. and Plunger, W. (1991) Evidence for episodic hydrothermal activity in the Red Sea, from the composition and formation of hydrothermal sediments, Thetis Deep. *Tectonophysics*, **190**, 109–117.

Schwertmann, U. (1959) Die fraktionierte Extraktion der freien Eiseoxyde in Boden, ihre mineralogischen Formen und ihre Entstehungsweisen. *Zeitschrift für Pflanzenernährung Düngung und Bodenkunde*, **84**, 194–204.

Schwertmann, U. (1964) Differenzierung der Eisenoxide des Bodens durch Extraktion mit Ammoniumoxalat-Lösung. *Zeitschrift für Pflanzenernährung Düngung und Bodenkunde*, **105**, 194–202.

Schwertmann, U., Cambier, P. and Murad, E. (1985) Properties of goethites of varying crystallinity. *Clays and Clay Minerals*, **33**, 369–375

Shanks III, W.C. and Bischoff, J.L. (1980) Geochemistry, sulfur isotope composition, and accumulation rates of Red Sea geothermal deposits. *Economic Geology and the Bulletin of the Society of Economic Geologists*, **75**, 445–459.

Taitel-Goldman, N. and Singer, A. (2001) High resolution transmission electron microscopy study of newly formed sediments in the Atlantis II Deep, Red Sea. *Clays and Clay Minerals*, **49**, 174–182.

Taitel-Goldman, N. and Singer A. (2002a) Metastable Si-Fe phases in hydrothermal sediments of Atlantis II Deep, Red Sea. *Clay Minerals*, **37**, 221–234.

Taitel-Goldman, N. and Singer, A. (2002b) Synthesis of clay-sized iron oxides under marine hydrothermal conditions *Clay Minerals*, **37**, 719–731.

Taitel-Goldman, N., Singer, A. and Stoffers, P. (1999) A new short range ordered, Fe-Si phase in the Atlantis II Deep, Red Sea hydrothermal sediments. Pp. 697–705 in: *Clays for our Future* (H. Kodama, A.R. Mermut and J.K. Torrance editors). Proceedings of the 11th International Clay Conference, Ottawa, Canada, 1997. Published by ICC97 Organizing Committee, Ottawa, Canada.

Taitel-Goldman, N., Bender Koch, C. and Singer, A. (2002) Lepidocrocite in hydrothermal sediments of the Atlantis II and Thetis Deeps, Red Sea. *Clays and Clay Minerals*, **50**, 186–197.

(*Received 16 May 2002; revised 31 July 2003; Ms. 661: A.E. Helge Stanjek*)